Supporting information

Room Temperature Exciton Formation and Robust Optical Properties of CVD-Grown Ultrathin Bi_2O_2Se Crystals on Arbitrary Substrates

Md Tarik Hossain[1] , Tadasha Jena[2], Upasana Nath[3], Manabendra Sarma[3] and P. K. Giri[1, 2♣]

[1]*Department of Physics, Indian Institute of Technology Guwahati, Guwahati -781039, India*

[2]*Centre for Nanotechnology, Indian Institute of Technology Guwahati, Guwahati 781039, India*

[3]*Department of chemistry, Indian Institute of Technology Guwahati, Guwahati 781039, India*

Index:

♣ Corresponding author, email: giri@iitg.ac.in (PKG),

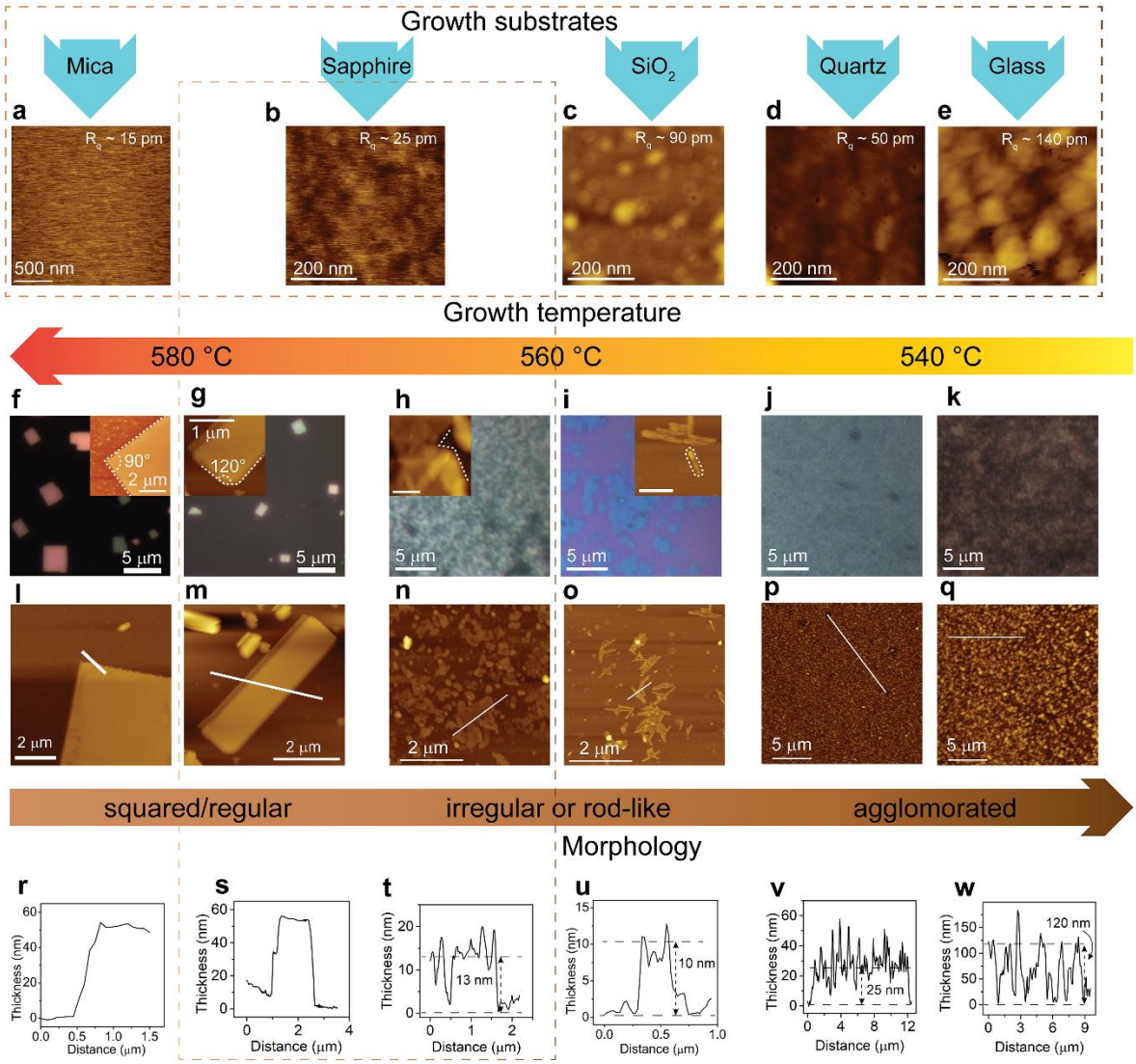

Figure S1: (a-e) Atomic force microscopy images of mica, sapphire, SiO_2, quartz, and glass substrate denoting the roughness of the surface. (f-k) Optical microscopy images of as-grown samples on different substrates. (j-q) Topography images of as-grown samples and (r-w) their corresponding height profile. Inset of (f-i) highlights the edge morphology of the synthesized Bi_2O_2Se. Inset of (h and i) has the scale bar of 0.2 and 0.5 μm.

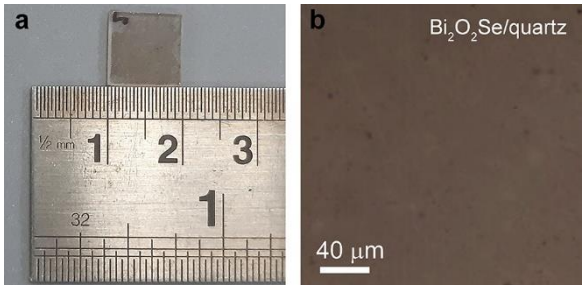

Figure S2: (a) Photograph of Bi_2O_2Se film grown over a 1×1 cm^2 quartz substrate. (b) Optical microscopy image of Bi_2O_2Se film over quartz substrate displaying large area growth.

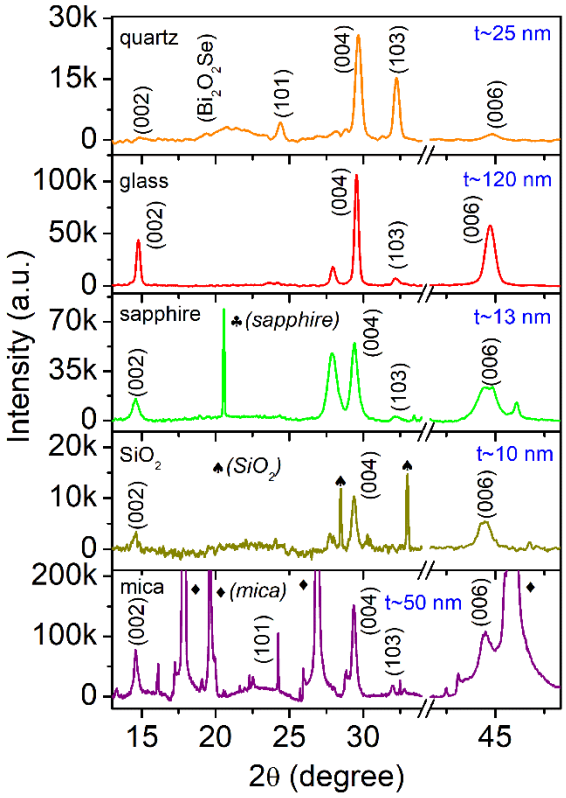

Figure S3: Comparative XRD pattern of Bi_2O_2Se crystals directly grown on mica, SiO_2, sapphire, glass, and quartz substrates by CVD process.

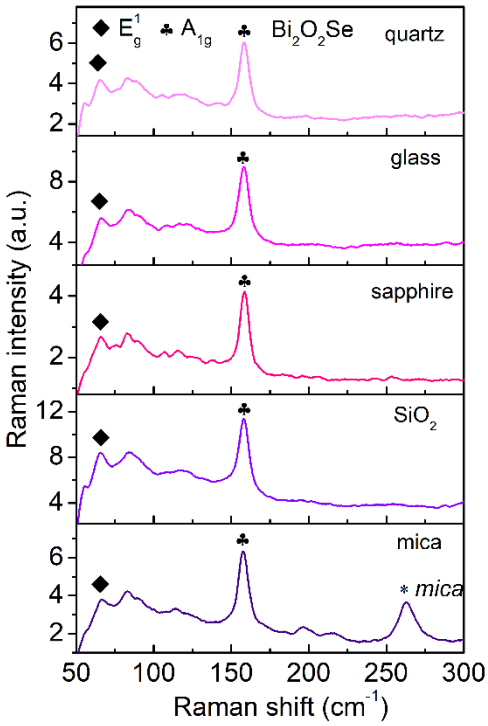

Figure S4: Comparative Raman spectra of Bi_2O_2Se crystals directly grown on mica, SiO_2, sapphire, glass, and quartz substrates by CVD process.

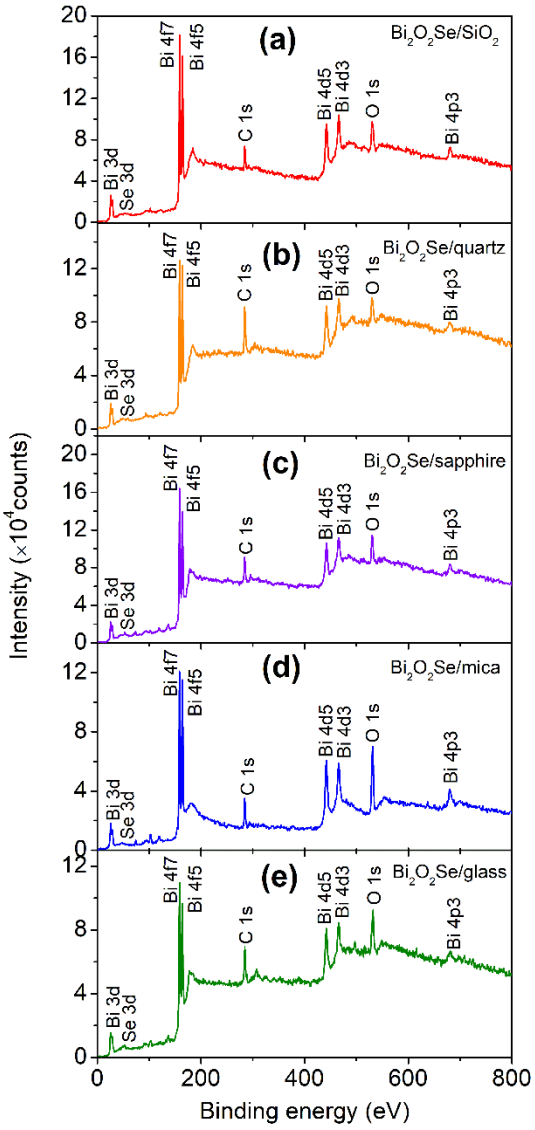

Figure S5: Comparative XPS survey scan spectra of Bi_2O_2Se on (a) Sapphire, (b) quartz, (c) SiO_2, (d) mica, and (e) glass substrates.

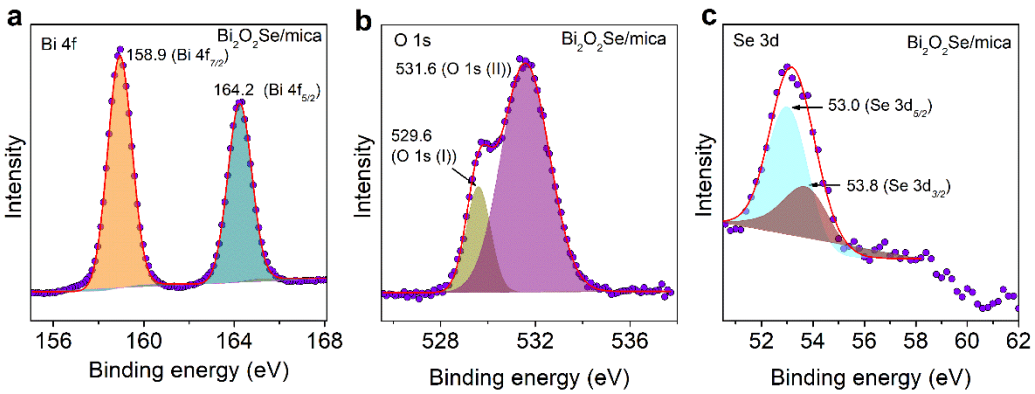

Figure S6: XPS spectra of Bi_2O_2Se on mica substrate: (a) Bi 4f, (b) O 1s, and (c) Se 3d. Experimental data are represented using symbols and fitted spectra using solid lines with shaded regions. Shirley's baseline was utilized for XPS spectral fitting.

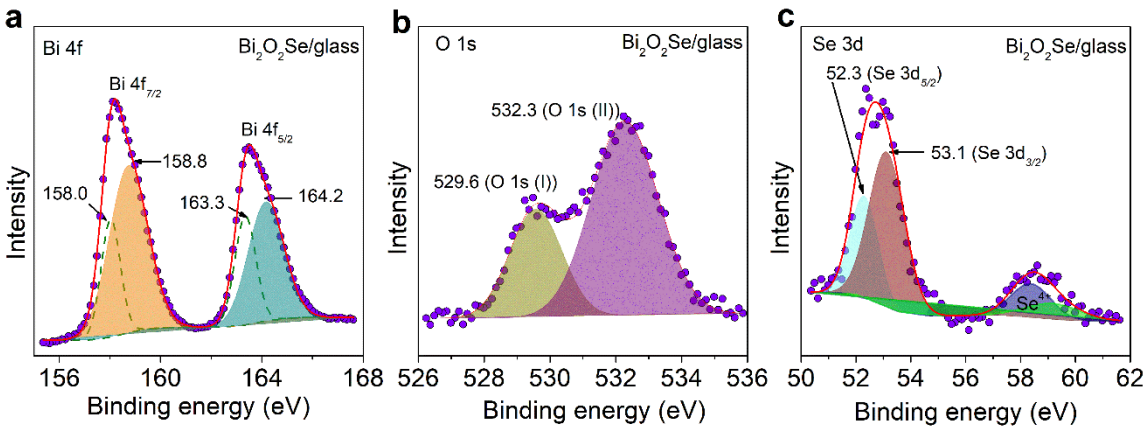

Figure S7: XPS spectra of Bi_2O_2Se on glass substrate: (a) Bi 4f, (b) O 1s, and (c) Se 3d. Experimental data are represented using symbols and fitted spectra using solid lines with shaded regions. Shirley's baseline was utilized for XPS spectral fitting.

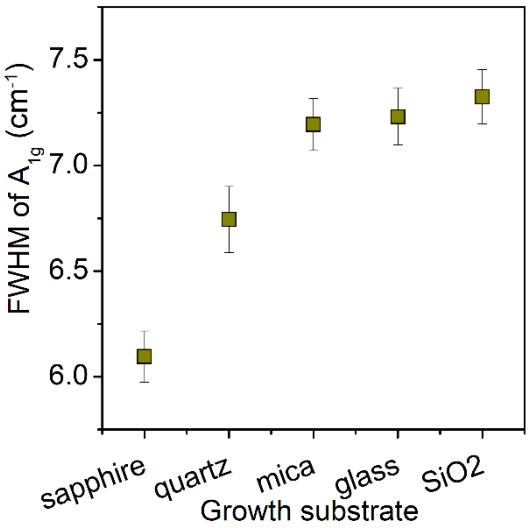

Figure S8: FWHM of Raman A_{1g} Raman mode of Bi_2O_2Se on different growth substrates.

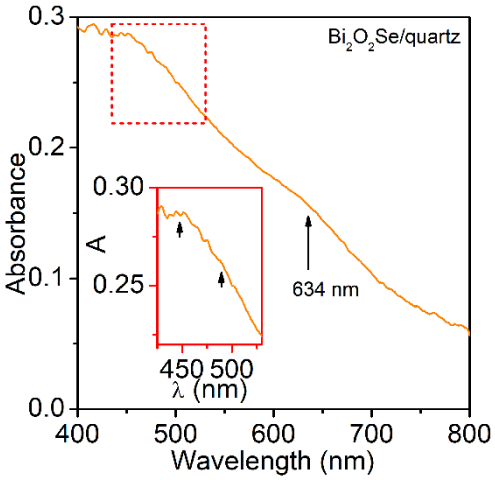

Figure S9: Absorption spectrum of Bi_2O_2Se on quartz substrate. The inset shows a magnified view of the absorption spectrum in the region 425-530 nm.

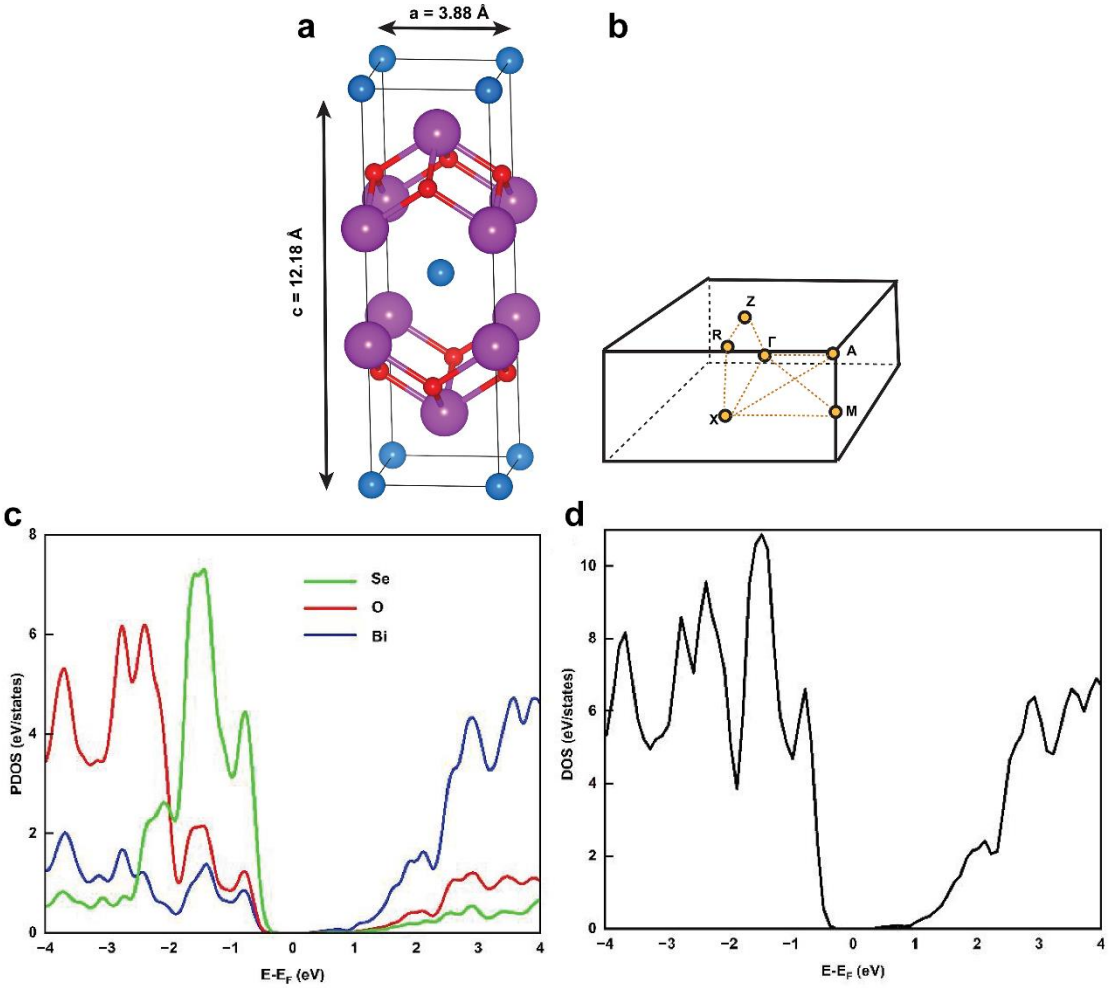

Figure S10: (a) Optimized structure (I4/mmm), (b) High symmetry K-point in the Brillouin zone, and (c) Partial Density of states (PDOS) of Bi, O, and Se. (d) Density of states (DOS) of Bi_2O_2Se. Purple, red, and blue balls depict Bi, O, and Se atoms, respectively. Fermi-level (E_F) is set at zero.

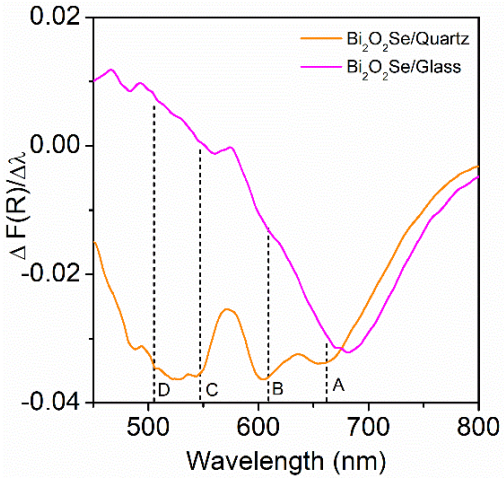

Figure S11: Differentiated Kubelka-Munk plot (absorption spectra) depicting multiple exciton peaks of Bi_2O_2Se grown on quartz and glass substrates.

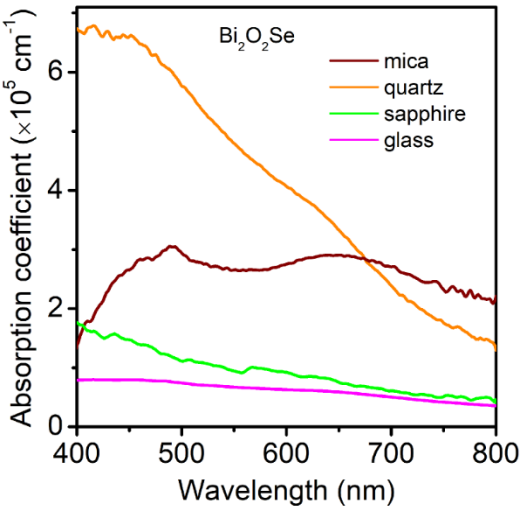

Figure S12: Absorption coefficients of Bi_2O_2Se grown on mica, quartz, sapphire, and glass substrates.

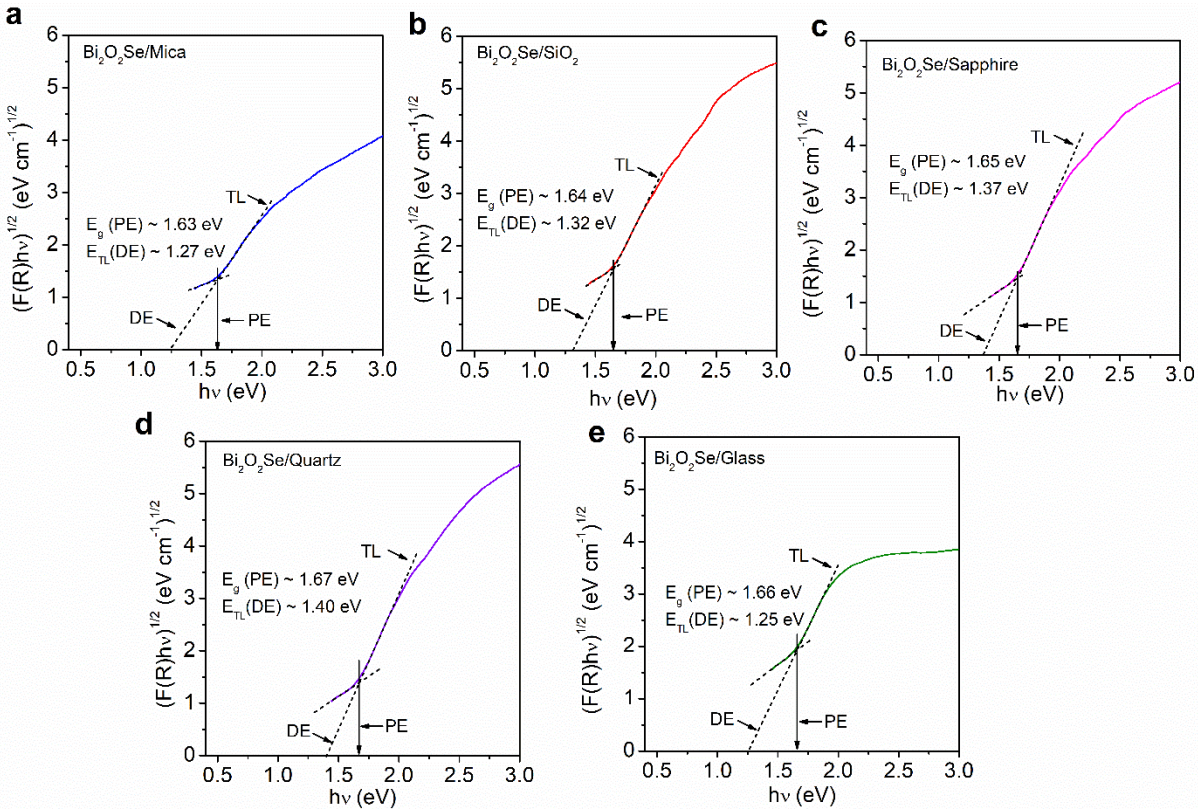

Figure S13: Tauc plot (indirect bandgap) of Bi_2O_2Se crystals on (a) mica, (b) SiO_2, (c) sapphire, (d) quartz, and (e) glass substrates. Direct extrapolation (DE) and proper extrapolation (PE) estimate of the optical energy gap of as-grown Bi_2O_2Se on different substrates.[1,2]

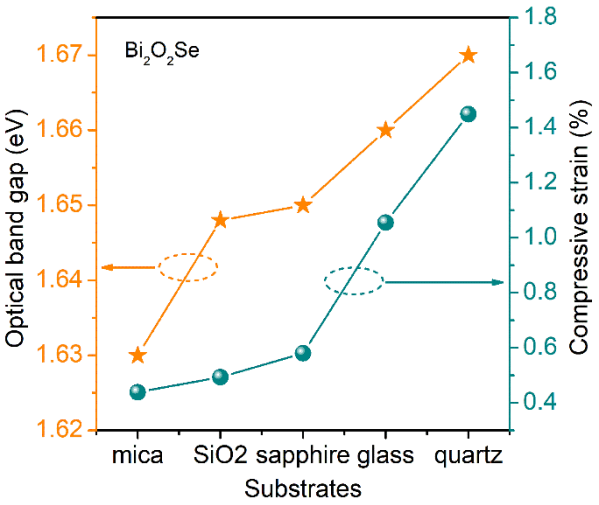

Figure S14: Direct correlation between the measured optical bandgap and strain in Bi_2O_2Se crystals on different substrate.

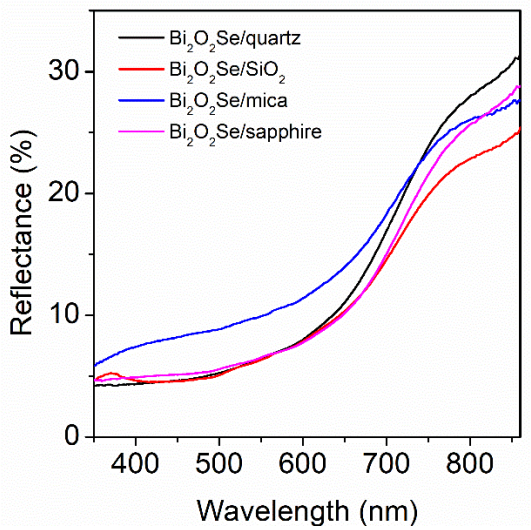

Figure S15: Reflectance spectra of Bi_2O_2Se crystals on mica, quartz, sapphire, and SiO_2 substrates.

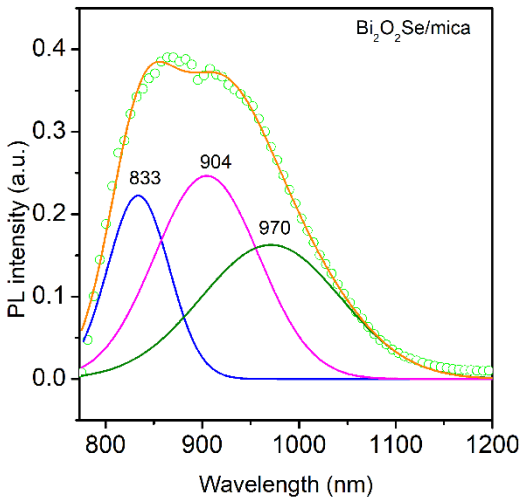

Figure S16: NIR PL spectra of Bi_2O_2Se crystals on mica substrates. The solid linesa are Gaussian fitted spectra showing 833, 904, 970 nm peaks originating from indirect transitions. Symbols represents the experimental data.

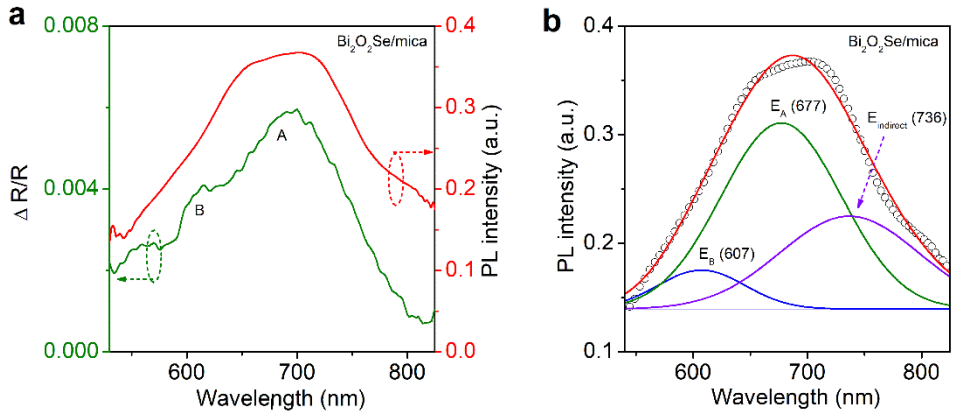

Figure S17: (a) Differential reflectance spectrum (left y-axis) and PL spectrum (right y-axis) of Bi_2O_2Se crystals grown on mica substrate. (b) Deconvoluted PL spectra of Bi_2O_2Se on mica.

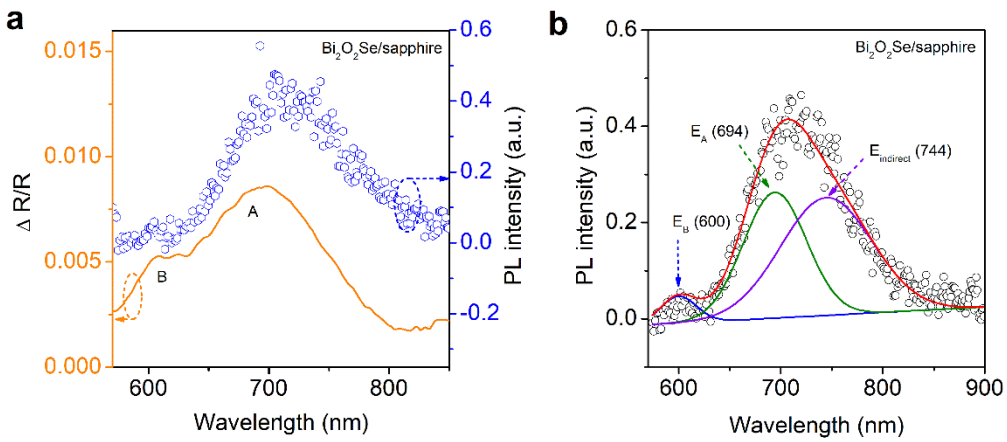

Figure S18: (a) Differential reflectance spectrum (left y-axis) and PL spectrum (right y-axis) of Bi_2O_2Se crystals grown on a sapphire substrate. (b) Deconvoluted PL spectra of Bi_2O_2Se on sapphire.

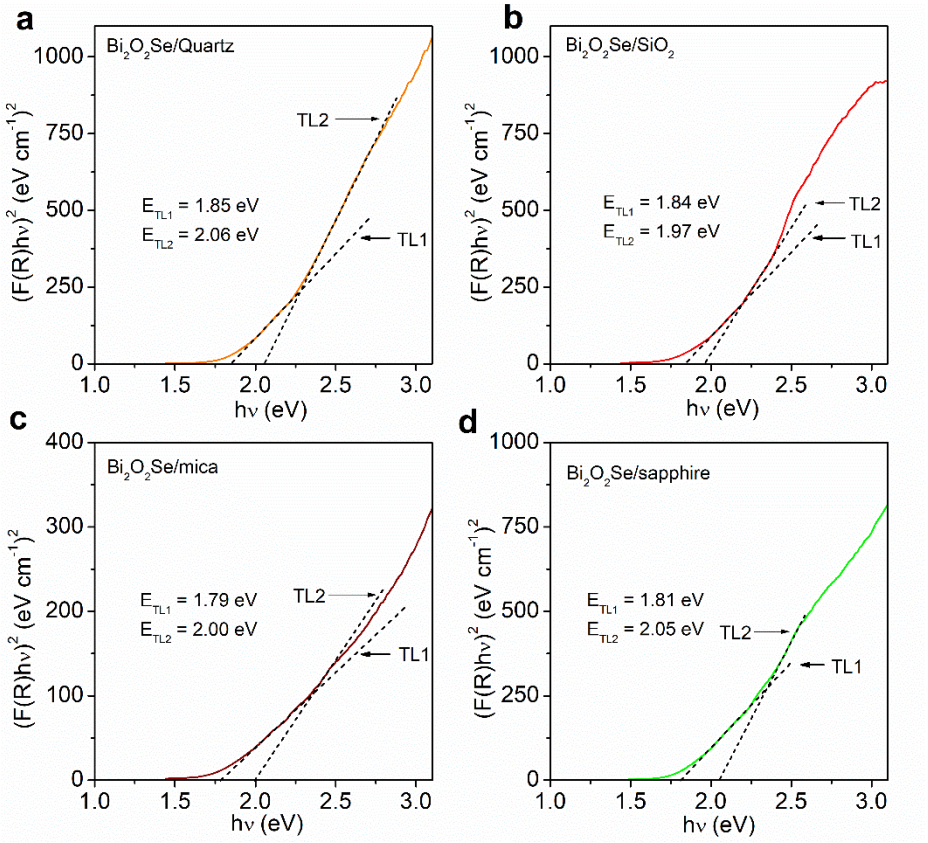

Figure S19: Tauc plot considering the direct band gap of Bi_2O_2Se crystals on (a) mica, (b) SiO_2, (c)sapphire, (d) quartz, and (e) glass substrates. Tauc line 1 (TL1) defines the first direct optical transition, while Tauc line 2 (TL2) signifies the second direct optical transition.

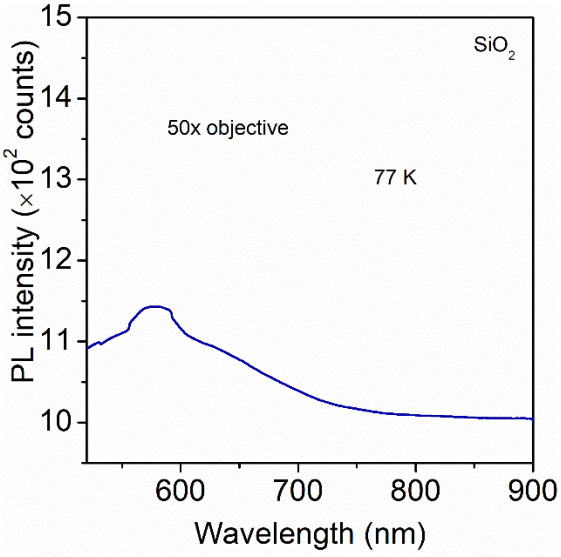

Figure S20: Low temperature (77 K) PL spectrum of bare SiO_2 substrate.

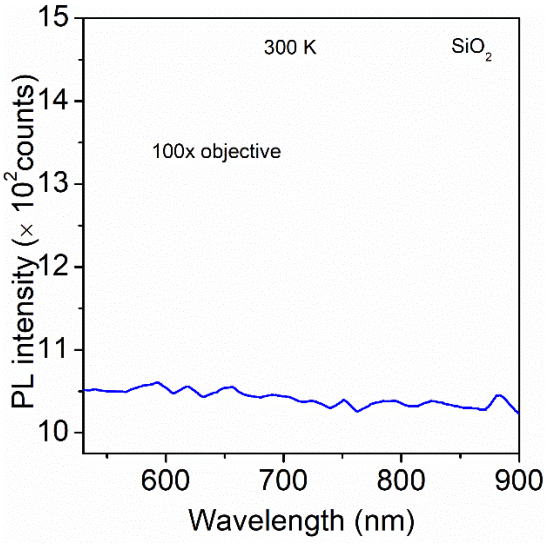

Figure S21: Room temperature (300 K) PL spectrum of bare SiO_2 substrate.

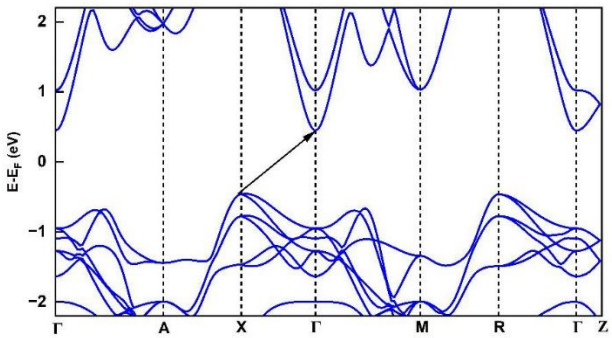

Figure S22: Electronic band structure plot of Bulk- Bi_2O_2Se using DFT+U.

Table S1: Fitting parameters of XPS spectra showing the binding energies of each element (Bi 4f, O 1s, Se 3d) in Bi_2O_2Se grown on different substrates.

Growth Substrate	Growth temperature (°C)	Binding energies (eV)							
		Bi		O1s		Se $^{2+}$		Se $^{4+}$	
		$4f_{7/2}$	$4f_{5/2}$	(I)	(II)	$3d_{5/2}$	$3d_{3/2}$	(I)	(II)
Sapphire	560	158.8	164.2	530.1	530.8	53.0	53.8	58.5	59.3
Quartz	540	159.0	164.3	529.9	531.5	53.1	53.8	58.6	59.4
SiO_2	560	159.2	164.5	530.0	531.9	52.8	53.7	58.8	59.9
Mica	560	158.9	164.2	529.6	531.6	53.0	53.8	-	-
Glass	540	158.8	164.2	529.6	532.3	52.3	53.1	58.4	59.2

Table S2: Absorption peak positions of Bi_2O_2Se for different growth substrates.

Growth Substrate	Peak positions (nm)
Mica	~460 nm, ~490 nm, ~654 nm
Glass	~456 nm, ~484 nm, ~649 nm
Quartz	~435 - 550 nm, ~634 nm
Sapphire	~450 nm, ~486 nm, ~651 nm
SiO_2	~455 nm, ~486 nm, ~662 nm

Table S3: 'Refractive index (*n*)' of as-grown Bi_2O_2Se and the growth substrates.

Growth substrate	***n* of growth substrate**	***n* of Bi_2O_2Se on the growth substrate**
Quartz	1.40	3.367
SiO_2	1.47	3.375
Glass	1.52	3.370
Mica	1.56	3.378
Sapphire	1.77	3.373

Table S4: Energy values at different high symmetry k-points, as obtained from the DFT calculation.

Valance Band (eV)		**Conduction Band (eV)**	
Γ_{VB} (outer)	-0.99	Γ_{CB} (outer)	0.87
Γ_{VB} (inner)	-1.36	Γ_{CB} (inner)	1.27
X_{VB}	-0.44	-	-
M_{VB}	-1.40	M_{CB} (outer)	1.23
-	-	M_{CB} (inner)	1.42
R_{VB}	-0.45	-	-
A_{VB}	-1.52	A_{CB}	2.13
Z_{VB}	-1.13	-	-

Table S5: Summary of energy differences at high symmetry k-points due to different indirect and direct transitions calculated theoretically and observed experimentally.

	Theoretical values			**Experimental values**
Transitions	**Energy (eV)**	**Wavelength (nm)**	**Exciton**	**Wavelength (nm)**
Γ_{VB} (outer)−Γ_{CB} (outer)	1.86	667	A	683
Γ_{VB} (inner)−Γ_{CB} (outer)	2.23	556	B	606
Γ_{VB} (outer)−Γ_{VB} (inner)	2.26	548	C	551
Γ_{VB} (inner)−Γ_{CB} (inner)	2.63	471	D	500
M_{VB}−M_{CB} (outer)	2.63	471		
M_{VB}−M_{CB} (inner)	2.82	440	E	
X_{VB}−Γ_{CB} (outer)	1.31	946	$E_{indirect}$	970
R_{VB}−Γ_{CB} (outer)	1.32	939		904
X_{VB}−M_{CB} (outer)	1.67	743		833
R_{VB}−M_{CB} (outer)	1.68	738		728
X_{VB}−Γ_{CB} (inner)	1.71	725		
R_{VB}−Γ_{CB} (inner)	1.72	721		
R_{VB}−M_{CB} (inner)	1.87	663		
Γ_{VB} (outer)−M_{CB} (outer)	2.22	559		
M_{VB}−Γ_{CB} (outer)	2.27	546		
Γ_{VB} (outer)−M_{CB} (inner)	2.41	515		
Γ_{VB} (inner)−M_{CB} (outer)	2.59	479		
M_{VB}−Γ_{CB} (inner)	2.67	464		
Γ_{VB} (inner)−M_{CB} (inner)	2.78	446		

References:

1 Jubu, P. R., Yam, F. K., Igba, V. M. & Beh, K. P. Tauc-plot scale and extrapolation effect on bandgap estimation from UV–vis–NIR data – A case study of β-Ga2O3. *Journal of Solid State Chemistry* **290**, 121576, doi:https://doi.org/10.1016/j.jssc.2020.121576 (2020).

2 Jubu, P. R. *et al.* Influence of the secondary absorption and the vertical axis scale of the Tauc's plot on optical bandgap energy. *Journal of Optics*, doi:10.1007/s12596-022-00961-6 (2022).